Composite Structures 286 (2022) 115326

Contents lists available at ScienceDirect

Composite Structures

journal homepage: www.elsevier.com/locate/compstruct

Improved electromagnetic wave shielding capability of carbonyl iron powder-embedded lightweight CFRP composites

Daeik Jang [a], B.H. Choi [a], H.N. Yoon [a], Beomjoo Yang [b], H.K. Lee [a,*]

[a] Department of Civil and Environmental Engineering, Korea Advanced Institute of Science and Technology (KAIST), 291 Daehak-ro, Yuseong-gu, Daejeon 34141, Republic of Korea
[b] School of Civil Engineering, Chungbuk National University, 1 Chungdae-ro, Seowon-gu, Cheongju, Chungbuk 28644, Republic of Korea

ARTICLE INFO

Keywords:
Electromagnetic wave shielding
Carbonyl iron powder
Carbon fiber-reinforced polymer
Lightweight
Frequency bandwidth

ABSTRACT

In the present study, carbonyl iron powder (CIP)-embedded carbon fiber-reinforced polymer (CFRP) composites were fabricated as lightweight electromagnetic interference (EMI) shielding composites. Four different CIP contents (e.g., 0%, 100%, 200%, and 300% by mass of epoxy resin) were added to fabricate the composites, and the effects of the incorporated CIP contents on the electrical characteristics and EMI shielding capability of the composites were investigated by means of AC conductivity, reflection and absorption of EM wave shielding tests, and by calculating the permittivity and permeability values. These outcomes showed that the EMI shielding capability was improved when increasing the incorporated CIP content. The results were analyzed using microstructural images taken via a FE-SEM and by EDS observations, which showed that the Fe-atomic components increased with the addition of CIP, thus improving the EMI shielding capability. In addition, the fabricated CIP-embedded CFRP composites were coated onto cement mortar and the applicability of these coated composites as EMI shielding composites in structures was examined. Shielding effectiveness exceeding 50 dB was noted, suggesting a potential of utilizing the fabricated CIP-embedded CFRP composites as EMI shielding composites in the structures.

1. Introduction

With the rapid developments of electrical devices and the increasingly widespread use of 5G telecommunication technology, the demand for electromagnetic interference (EMI) shielding composites has strengthened due to the harmful effects of EMI on people's health [1]. In addition, unnecessary electromagnetic (EM) waves can interfere with other electrical communication devices, increasing the importance of EMI shielding composites in the communications industry [2–5]. In civil engineering fields, construction equipment and structures are susceptible to EM waves; thus, cement-based barriers composed of metallic materials are widely used as EMI shielding composites for the protection from the EM waves [5–7]. However, the incorporation of conventional metallic materials into the cement-based barriers can increase the weight and lead to corrosion problems, thus presenting various obstacles that prevent the wider application of these materials in civil industries [6–8].

For these reasons, many researchers have attempted to utilize the carbon-based materials (e.g., carbon fiber, carbon black, and carbon nanotube) to cement-based barriers given their excellent electrical conductivity which renders EMI shielding properties to the barriers [6–15,39,40]. Nam et al. [6] incorporated 1.0 wt% multi-walled nanotube into 2.36 mm cementitious composites, showing EMI absorption shielding effectiveness of 29 dB in a frequency range of 8.2 to 12.0 GHz. Micheli et al. [16] fabricated 3 cm concrete composites incorporating 3 wt% carbon nanotube, with the composites showing EMI shielding effectiveness of approximately 12 dB at an input frequency of 2.6 GHz. Yoon et al. [13] added CNT 0.2% and CF 0.5% with length of 6 mm to the cementitious composites, and the composites exhibited 18 dB of EMI shielding effectiveness at an input frequency of 10 GHz. Although many researchers have investigated the potential utilization of carbon-based materials as EMI shielding composites, various obstacles such as dispersion and their high cost have led to low applicability of these materials in civil industries.

In recent years, carbonyl iron powder (CIP), with a purity level of 97%, has been highlighted in relation to the fabrication of EMI shielding composites due to its outstanding magnetic properties and high saturation magnetization characteristics [17–23,35]. Chen et al. [17]

* Corresponding author.
E-mail address: haengki@kaist.ac.kr (H.K. Lee).

https://doi.org/10.1016/j.compstruct.2022.115326
Received 14 July 2021; Accepted 27 January 2022
Available online 1 February 2022

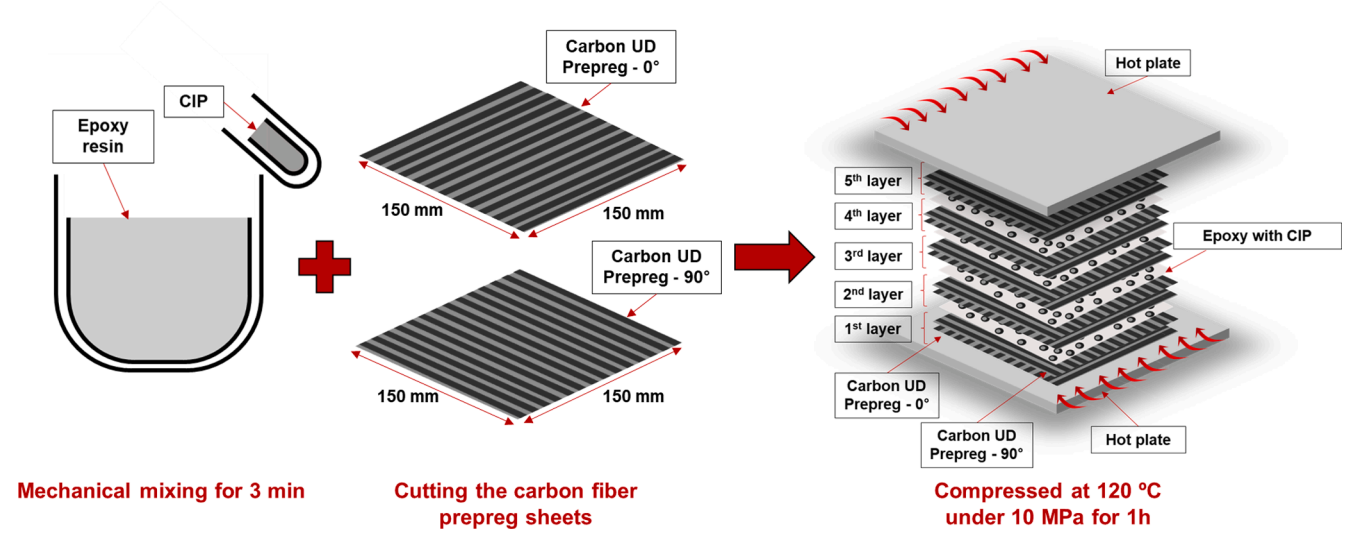

Fig. 1. Fabrication details of CIP-embedded CFRP composites.

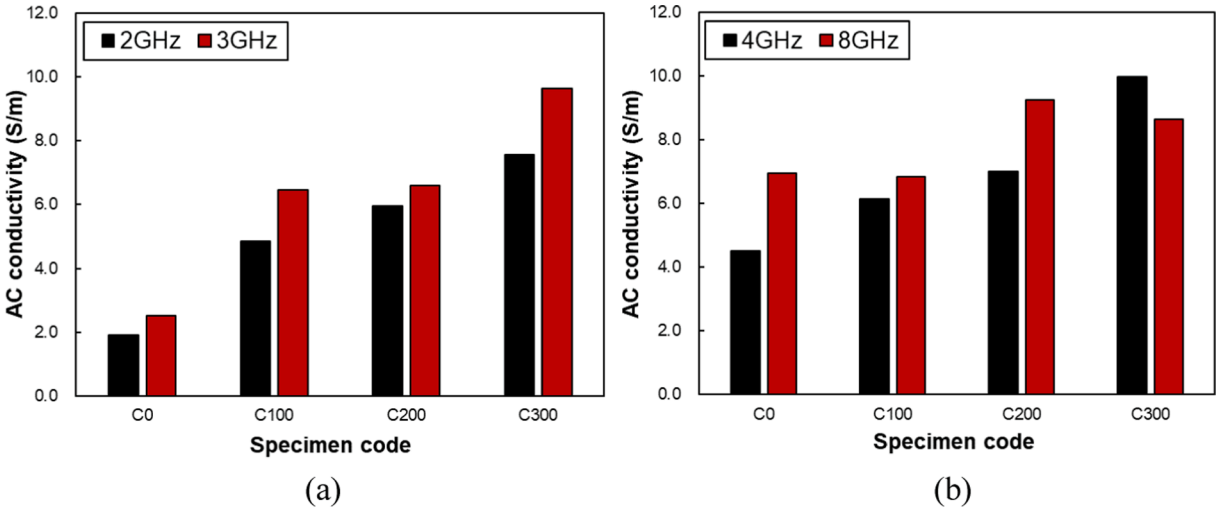

Fig. 2. AC conductivity of specimens in the (a) S-band and (b) C-band frequency ranges.

investigated the EMI shielding characteristics of CIP-incorporated epoxy composites, finding that increasing the CIP content has a notable effect on the EMI shielding effectiveness. Sedlacik et al. [19] fabricated polymeric composites incorporating CIP 40 vol% and observed that the fabricated composites showed EMI shielding effectiveness of approximately 20 dB. Sum et al. [21] examined the effects of the CIP concentration on the EMI shielding effectiveness of CIP-embedded cementitious composites. They found that the EMI reflection shielding effectiveness was increased from 2 dB to 17 dB when CIP 0.5 wt% was embedded into the cementitious composites, clearly demonstrating the potential of using CIP as an EMI shielding composite material in civil industries [21]. Although many efforts have demonstrated the notable effects of CIP incorporation that improve the EMI shielding capabilities of cementitious composites in civil industries, incorporating CIP into the cementitious composites is also associated with various disadvantages, such as a high cost and poor applicability to the existing structures.

In this regard, the present study focuses on the CIP-embedded carbon fiber-reinforced polymer (CFRP) composites. Lightweight CIP-embedded CFRP composites with high mechanical properties can readily attach to the cement-based structures. Moreover, CFRP composites are commonly utilized as the reinforcement composites in civil structures due to their high compatibility with the structures used in construction [24–26,38]. Herein, CIP amounts at four different concentrations (0, 100, 200, and 300 wt%) were added into an epoxy resin and were then coated onto carbon fiber sheets to fabricate the CIP-embedded CFRP composites. The AC conductivity, reflection and absorption shielding effectiveness, permittivity, and permeability of the fabricated composites were investigated to observe the effects of the CIP concentration on the EMI shielding capabilities. In addition, microstructural analyses of the fabricated composites were conducted by means of scanning electron microscopy (FE-SEM) and energy disperse X-ray spectroscopy (EDS). Lastly, the fabricated CIP-embedded CFRP composites were coated onto the cementitious composites and the applicability of the proposed composites as EMI shielding composites in civil structures was investigated.

2. Fabrication and measurements

2.1. Materials and fabrication procedure

In the present study, a 12 k carbon fiber UD prepreg (CP300NS), epoxy resin (L-101(R)), and CIP (CIP 3189) were utilized to fabricate the CIP-embedded CFRP composites for EMI shielding. The diameter of the CIP used here ranged from 3.0 to 4.0μ m and the purity was

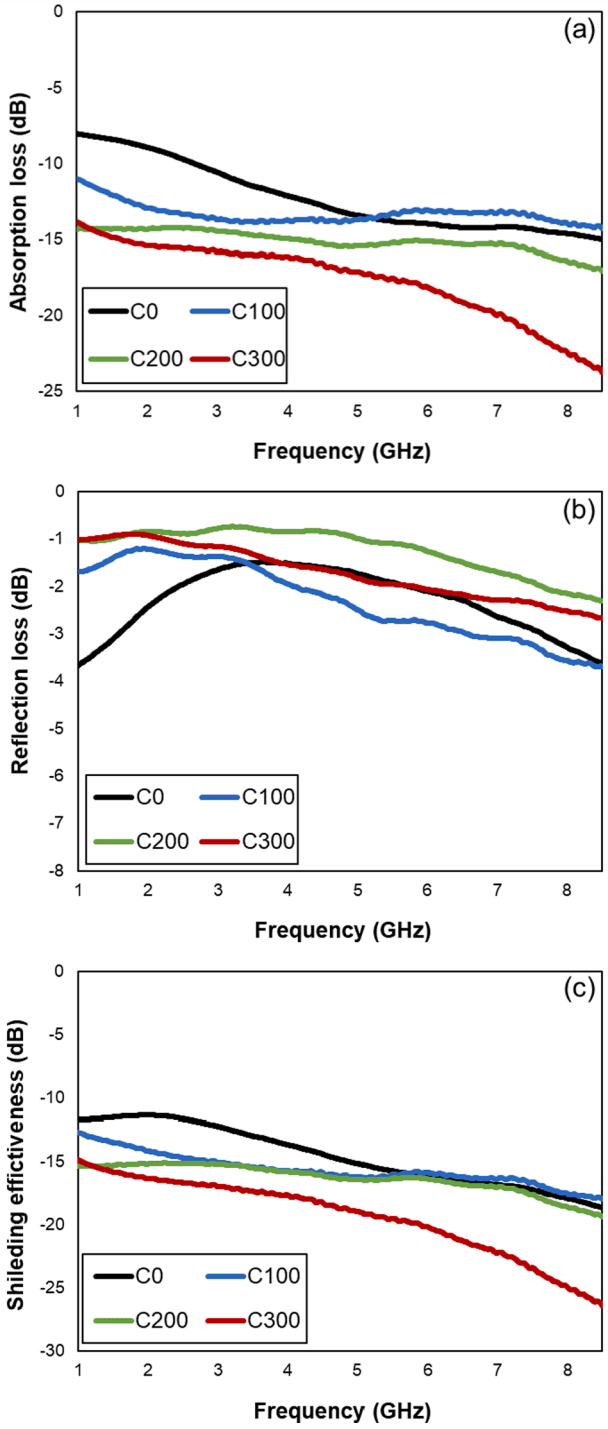

Fig. 3. Absorption (a), reflection (b), and total EMI shielding capabilities (c) of the specimens.

approximately 98%. The fabrication details of the CIP-embedded CFRP composites are shown in Fig. 1. CIP at levels of 0, 100, 200, and 300% by mass of epoxy resin was added into the epoxy resin to create four specimens, which were then mixed by hand for 3 min while the carbon fiber sheet used here was cut into pieces 150 × 150 mm^2 in size. Carbon fiber sheets rotating at angles of 0° and 90° were put into a mold and the epoxy resin with CIP was poured on the carbon fiber sheets to create a single layer (See Fig. 1).

An identical process was repeated for five cycles to build five layers, and the layered composites were compressed at 120 °C under 10 MPa for 1 h to fabricate the CIP-embedded CFRP composites [15]. The fabricated specimens are denoted here as C0, C100, C200, and C300 according to the incorporated CIP content. To measure the EMI shielding effectiveness of the specimens, they were cut into donut-shaped pieces with an inner diameter of 3 mm, outer diameter of 7 mm, and thickness of 4 mm [6,8,27]. Specimens for measurements of the tensile strength and Young's modulus were also prepared as confirming to ASTM D638. Meanwhile, a cement mortar sample 300 × 300 × 100 mm^3 in size was fabricated and the fabricated CFRP composites with 300% CIP were coated onto the cement mortar to assess the applicability of the specimens as EMI shielding composites in civil structures.

2.2. Experimental details

The electrical AC conductivity of the specimens was measured using a PNA-L network analyzer (Agilent N5239), a device capable of measuring the AC conductivity in the frequency range of 300 kHz to 8.5 GHz. The EMI shielding capabilities including four different S-parameters (i.e., S_{11}, S_{12}, S_{21}, S_{22}), the permittivity, and the permeability values were measured in the frequency range of 1.0 GHz and 8.9 GHz using a network analyzer, a 7-mm airline instrument (Agilent 85051), and materials measurement software (Agilent 85071E).

The tensile strength and Young's modulus of the specimens were measured using a universal testing machine (INSTRON 5982) with a loading rate of 2 mm/min. Five specimens in each of the mix proportions underwent the tensile strength testing; the average values were calculated from triplicate trials, except for the specimens with the maximum and minimum values. Microstructural images of the specimens were taken via a field emission FE-SEM (Hitachi SU 5000) [36,37]. In addition, the applicability of the specimens to civil structures was investigated, conforming to the military standard MIL-STD-188–125 [16] pertaining to sending and receiving antennas (Anritus) in the frequency bandwidth range of 600 MHz to 2 GHz. The receiving antenna in this case was placed in a shielding room with an absorber to minimize EM waves, and the shielding specimens were placed between the sending and receiving antennas at distances of 2 m and 1 m.

3. Results and discussions

3.1. Electrical conductivity and EMI shielding capability

The AC conductivity values of the specimens at the frequency ranges of S-band (2 GHz−3 GHz) and C-band (4 GHz−8 GHz) are shown in Fig. 2. This figure shows that the incorporation of CIP increased the AC conductivity, as indicated by the properties of the CIP. As reported in the literature, higher AC conductivity can be obtained by increasing the incorporated CIP content, showing a phenomenon similar to that found in a previous study [28]. In addition, the figure shows that the AC conductivity values are proportional to the applied input frequencies. According to earlier work, the AC conductivity of composites incorporating an electrical conductive filler is proportional to the frequency of the applied voltage, conforming to the Jonscher universal power law and suggesting a possible mechanism to explain the results in Fig. 2 [29,30].

Meanwhile, the EMI shielding capabilities against absorption loss and reflection loss and the overall shielding effectiveness of the specimens are shown in Figs. 3 and 4. The EMI shielding capabilities increased as the incorporated CIP content was increased, as indicated by the properties of CIP, which improved the conductivity and magnetization [17]. Specifically, it should be noted that the absorption loss is a more dominant factor with regard to the overall shielding effectiveness compared to the reflection loss, as shown in Fig. 4. Al-Saleh et al. [4] reported that the reflection loss serves as a primary shielding mechanism when shielding composites are composed of a sheet of a homogeneous conductive material, as opposed to composites with conductive fillers and an inclusive matrix. In contrast, the absorption loss is the main shielding mechanism in the composites composed of electrically

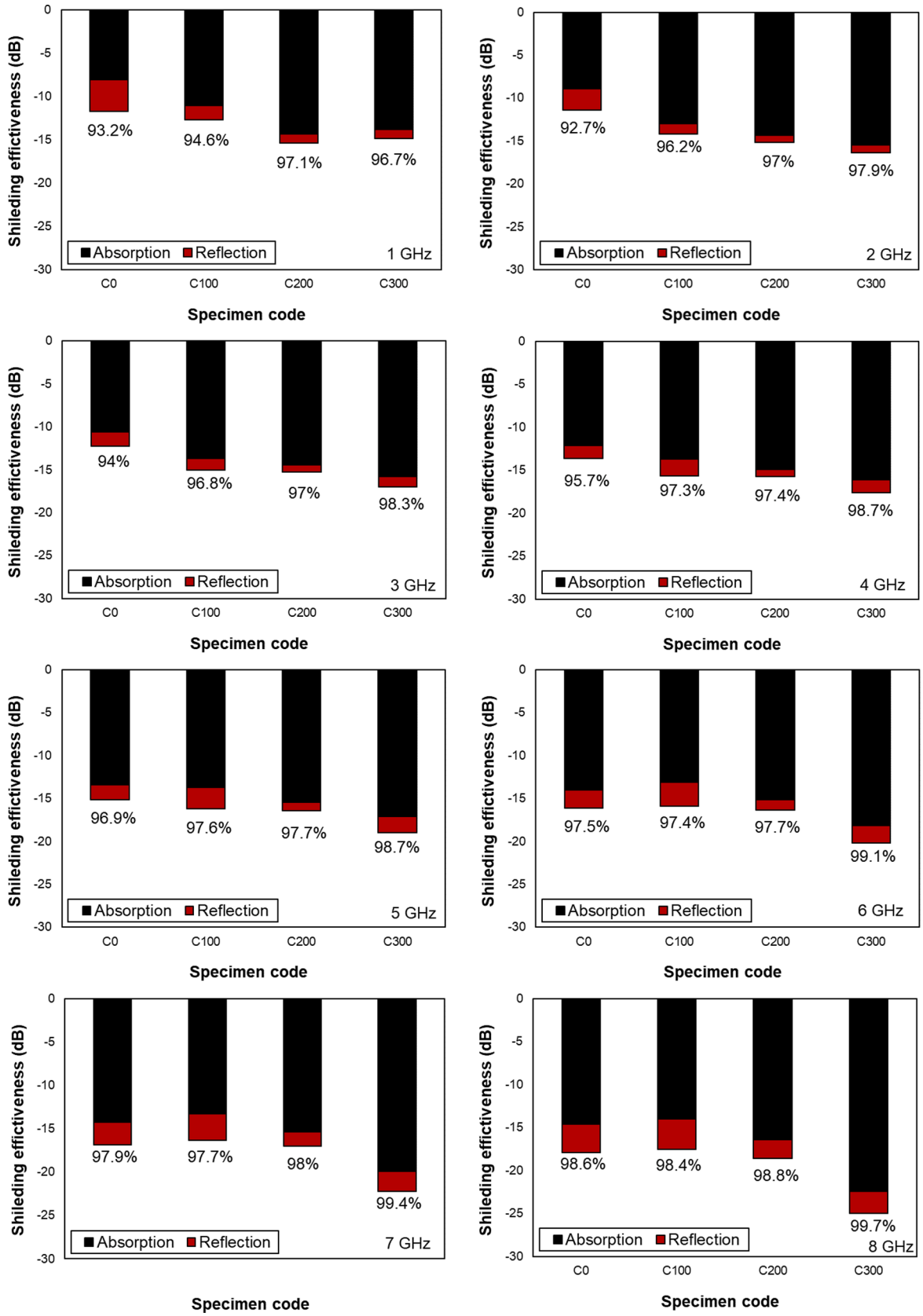

Fig. 4. EMI shielding effectiveness of the specimens in terms of absorption and reflection in representative frequencies.

Table 1
Shielding effectiveness at bandwidths of −10 dB, −15 dB, −20 dB, and −25 dB.

Shielding Effectiveness	Specimen code			
	C0	C100	C200	C300
−10 dB Band	1.0–8.5 GHz Width : 7.5 GHz	1.0–8.5 GHz Width : 7.5 GHz	1.0–8.5 GHz Width : 7.5 GHz	1.0–8.5 GHz Width : 7.5 GHz
−15 dB Band	4.9–8.5 GHz Width : 3.6 GHz	3.0–8.5 GHz Width : 5.5 GHz	1.0–8.5 GHz Width : 7.5 GHz	1.0–8.5 GHz Width : 7.5 GHz
−20 dB Band	–	–	–	5.9–8.5 GHz Width : 2.6 GHz
−25 dB Band	–	–	–	8.1–8.5 GHz Width : 0.4 GHz

conductive fillers and/or magnetic dipoles, and the absorption loss can be enhanced as materials with conductive and/or magnetic properties are incorporated into composites [4]. For these reasons, the absorption loss shows a higher value compared to those of the reflection loss, and the EMI shielding effectiveness improved as the incorporated CIP content was increased, exhibiting shielding effectiveness of 99.7% in the C300 specimen at 8 GHz (See Fig. 4).

The shielding effectiveness outcomes at bandwidths of −10, −15, −20, and −25 dB for the specimens are presented in Table 1. This table indicates that the incorporation of CIP improved the shielding effectiveness and widened the frequency bandwidth. Specifically, the C300 specimen showed shielding effectiveness of −20 dB at frequencies ranged from 5.9 to 8.5 GHz and of −25 dB at frequencies ranging from 8.1 to 8.5 GHz, with bandwidths of 2.6 and 0.4 GHz, respectively. The obtained bandwidths belong to the C-band; thus, these results exhibit an enlarged bandwidth compared to those reported in previous studies [6,7,31–33].

3.2. Permittivity and permeability values

The real and imaginary parts of the permittivity and permeability values were measured and were converted to loss factor values using a tangent function, as shown in Fig. 5. This figure shows that the loss factor of the permittivity has a higher value than that of the permeability. This can be deduced from the properties of the specimens composed of CFRP and CIP, leading to an improvement of the permittivity compared to the permeability [17]. Specifically, negative values were found for the permeability loss factor, as shown in Fig. 5, regardless of the specimen. Based on the theoretical background, the real and imaginary parts of the permeability are positive values, leading to the positive values of the loss factor [4]. However, some experimental values of the permeability showed negative values close to 0, indicating that negative values of the loss factor can be negligible.

In addition, the frequency-dependent properties of the permittivity-based loss factor were observed in the specimens incorporating CIP (i.e., C100, C200, and C300 specimens), and the periodic properties of the permittivity-based loss factors increased as the incorporated CIP content was increased. According to a study by Sum et al. [21], the periodic property can be determined by assessing the EMI shielding capability with composites composed of magnetic particles, leading to a resonance frequency, and an increase in the bandwidth related to EMI shielding capabilities can be realized. Hence, the results in Fig. 5 are in good agreement with earlier work, demonstrating the positive effects of CIP

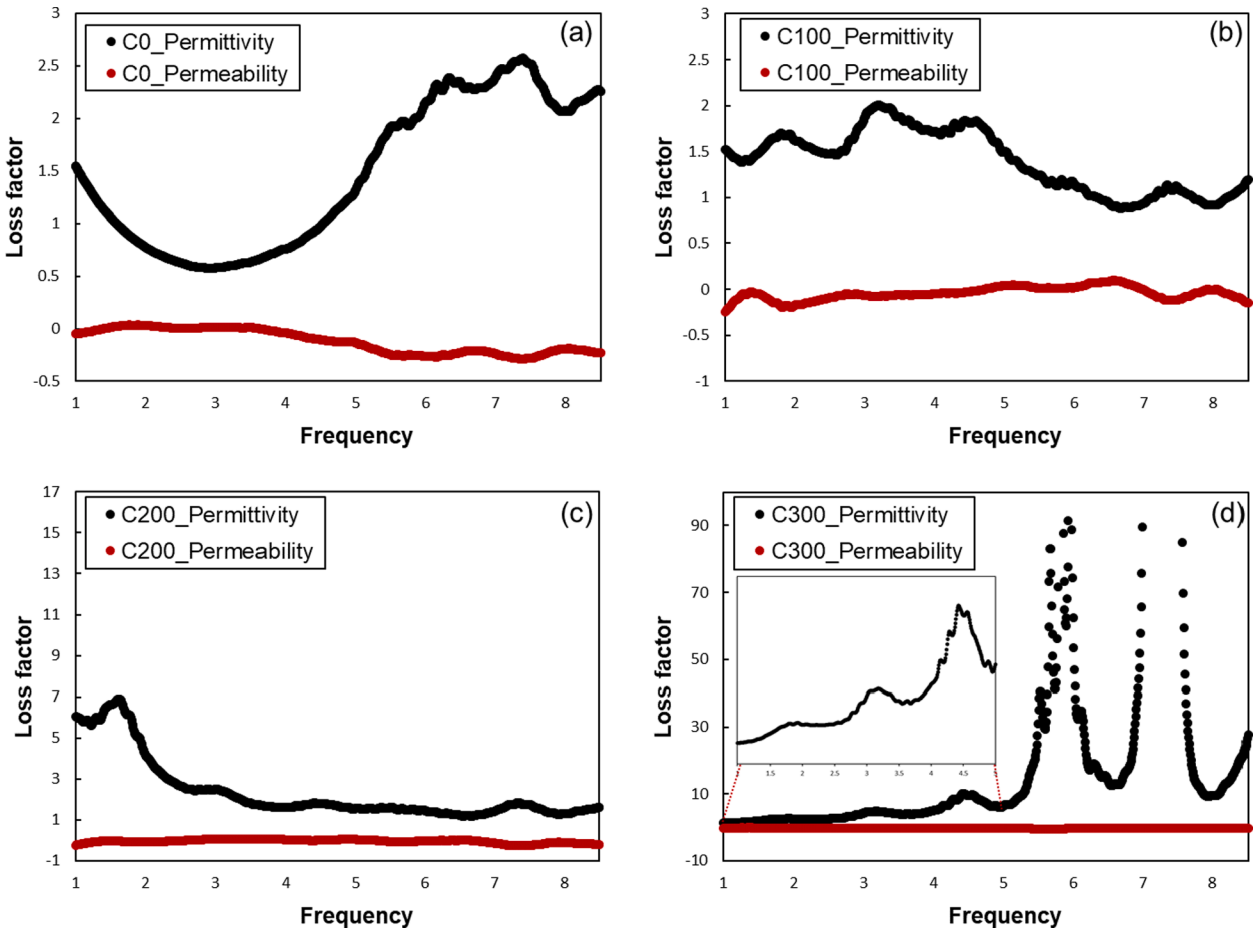

Fig. 5. Loss factor of the permittivity and permeability values: (a) C0, (b) C100, (c) C200 and (d) C300 specimens.

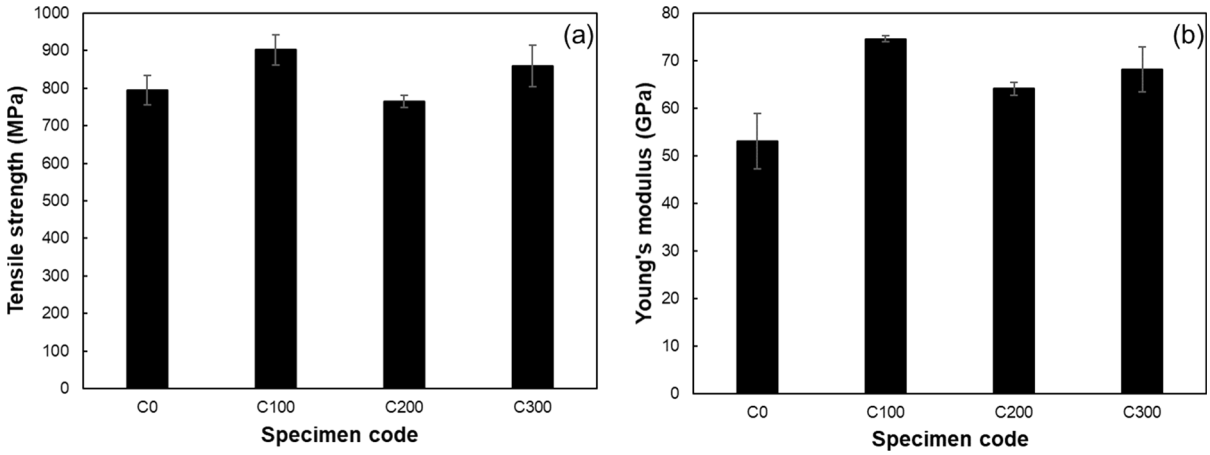

Fig. 6. Tensile strength (a) and Young's modulus (b) of the specimens.

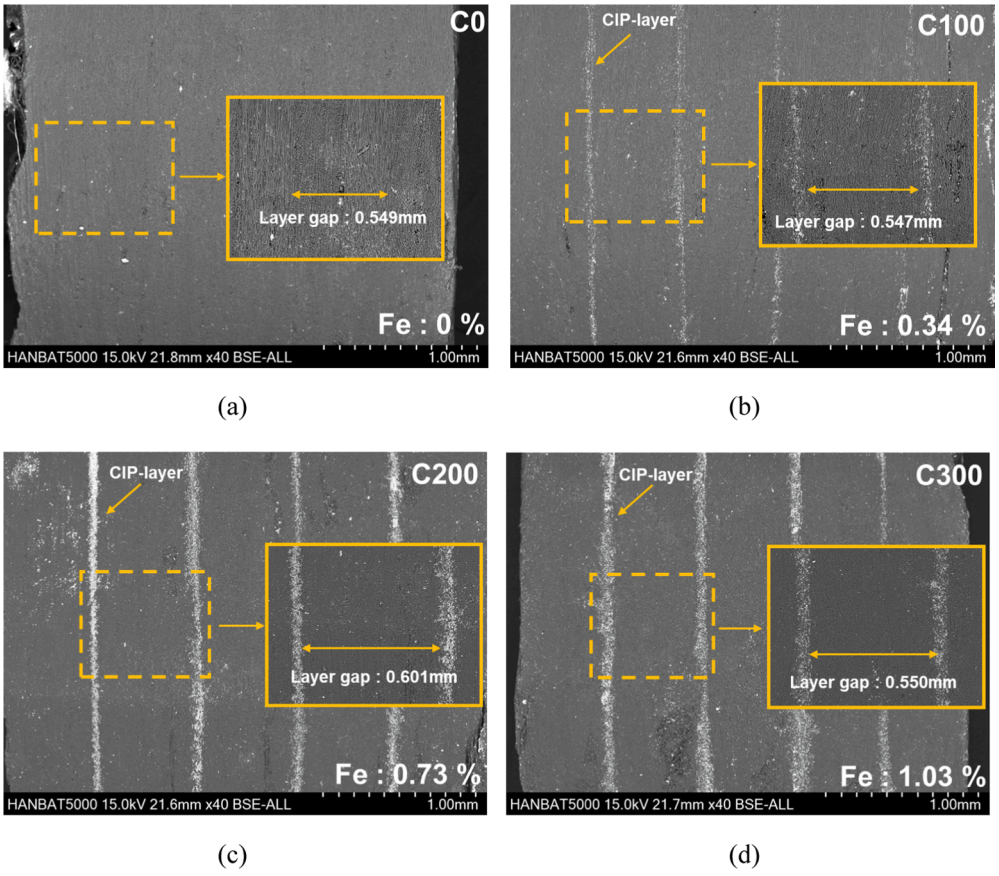

Fig. 7. SEM and EDS images of the (a) C0, (b) C100, (c) C200, and (d) C300 specimens with Fe atomic signals.

incorporation to improve the EMI shielding capabilities.

3.3. Mechanical properties and microstructural analysis

The tensile strength and Young's modulus values of the specimens are exhibited in Fig. 6. The specimens, regardless of the amount of incorporated CIP content, showed tensile strength and Young's modulus values that exceeded 750 MPa and 50 GPa, respectively. In addition, phenomena indicating that the incorporation of CIP increased the tensile strength and Young's modulus can be observed in Fig. 6, as determined from the CIP given its high mechanical properties. To analyze the small reduction in the tensile strength found in the C200 specimen, FE-SEM images were taken and the gaps between the CIP layers were measured.

As shown in Fig. 7, the gaps in the specimens were 0.549, 0.547, 0.601, and 0.550 mm as the CIP content was increased. The C200 specimen showed a gap wider than those of the other specimens, leading to lower tensile strength of the C200 specimen. Meanwhile, EDS observations were utilized to detect the Fe-atomic components in the specimens as the incorporated CIP content was increased. The Fe-atomic components were found to be 0, 0.34, 0.73, and 1.03 atomic% in the C0, C100, C200, and C300 specimens, respectively, as can be deduced from the incorporated CIP, which is composed of 97% of Fe-component. In this regard, the FE-SEM and EDS observation results in Fig. 7 are in agreement with results of the EMI shielding capability tests shown in

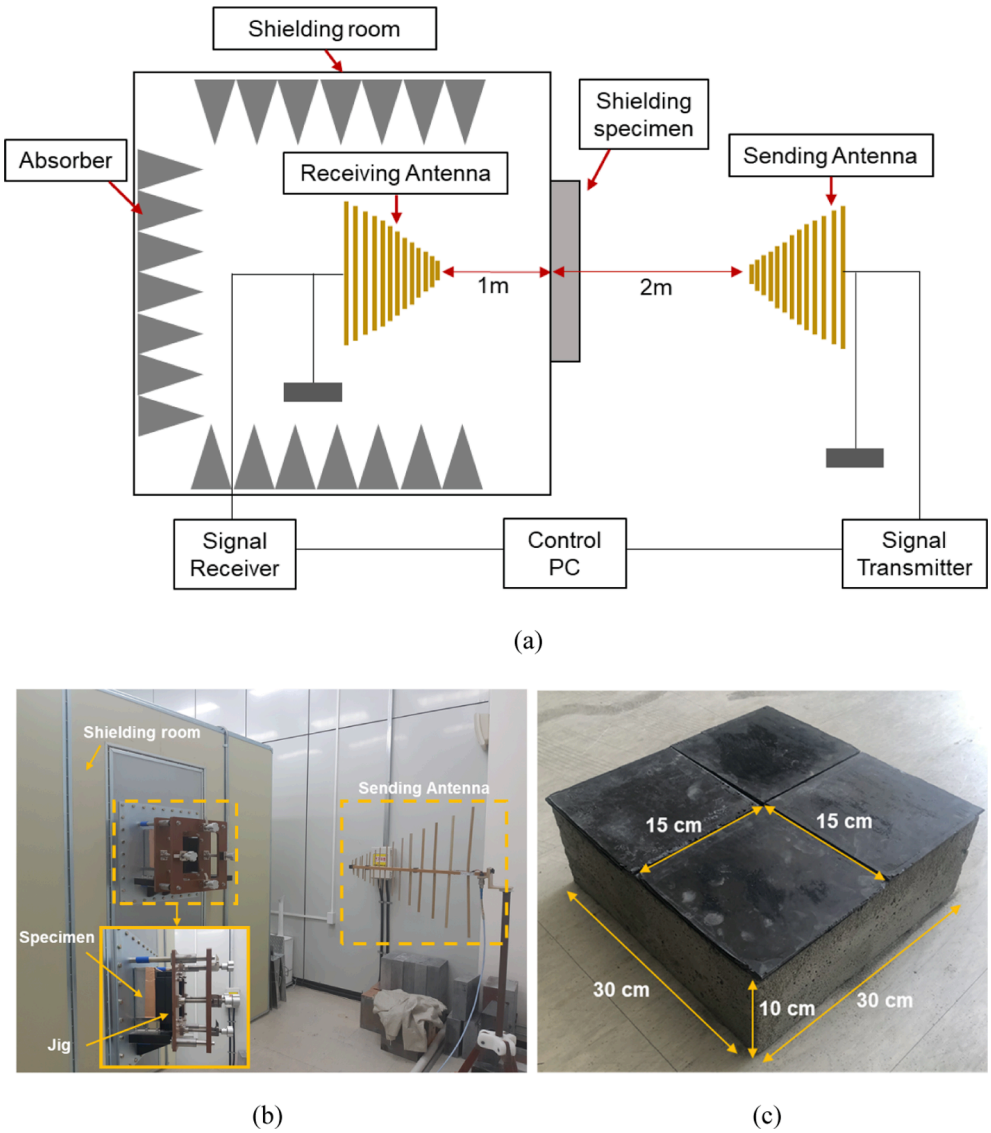

Fig. 8. Schematic description (a), experimental setup (b) for the mock-up test, and the utilized shielding specimens (c).

Figs. 3 and 4.

3.4. EMI shielding capability of cement mortar coated with CIP-embedded CFRP

A schematic description and the experimental setup used in the test are shown in Fig. 8 [34]. Here, a cement mortar was fabricated conforming to ASTM C1329, and the C300 specimens were chosen to be coated onto the cement mortar as a test of the EMI shielding capability, as shown in Figs. 3 and 4. One layer and three layers of the C300 specimen materials were coated onto the cement mortar, referred to here as the C300-1 layer and the C300-3 layer specimens. The shielding effectiveness of these coatings was compared to that of a cement mortar which served as a control specimen.

The horizontal and vertical shielding effectiveness of the specimens and their shielding effectiveness outcomes at 1 GHz and 2 GHz are exhibited in Fig. 9. This figure shows that the shielding effectiveness was improved when the C300 specimens were coated onto the cement mortar, and an increase of the number of layers led to an improvement of the shielding effectiveness. The control specimens exhibited horizontal and vertical shielding effectiveness outcomes of 5.8 dB and 6.0 dB, respectively, at an applied frequency of 1 GHz. However, the C300-1 layer and C300-3 layer specimens exhibited horizontal and vertical shielding effectiveness outcomes of 39.1 and 45.1, and 52.5 and 54.5 dB, respectively. Similarly, the horizontal and vertical shielding effectiveness values of the control, C300-1 layer, and C300-3 layer specimens were 6.7, 6.2, 40.6, 42.5, 50.5, and 49.0 dB. Hence, the C300-1 layer and C300-3 layer composites showed an improvement in the horizontal and vertical shielding effectiveness outcomes of approximately 579, 648, 812, and 805% at applied frequencies of 1 GHz, and 507, 586, 656, and 691% at an applied frequency of 2 GHz compared to those of the control specimen.

4. Concluding remarks

In the present study, CIP-embedded CFRP composites were fabricated with four different CIP contents (i.e., 0, 100, 200, and 300 wt%), and effects of CIP inclusion on the electrical and EMI shielding characteristics of the specimens were investigated. Microstructural images were taken to observe the Fe-atomic components in the specimens with an increase in the incorporated CIP contents. The main conclusions obtained from the present study are summarized below.

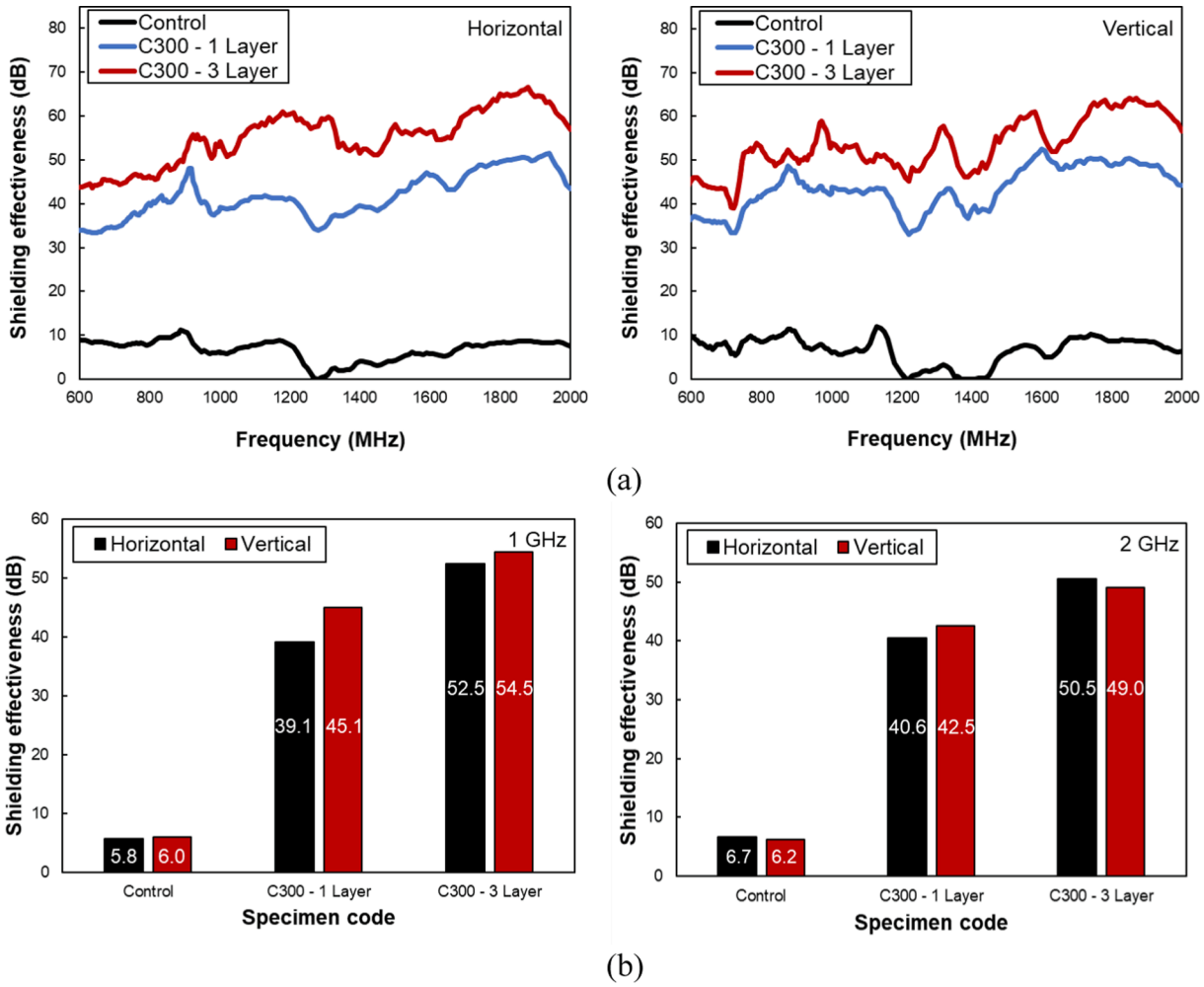

Fig. 9. Horizontal and vertical shielding effectiveness (a) and shielding effectiveness at 1 GHz and 2 GHz (b).

(1) The AC conductivity of the specimens was improved as the incorporated CIP content was increased, and the effects of incorporating CIP on the AC conductivity were dominant in the S- and C-band frequency ranges.
(2) Enhanced EMI shielding effectiveness of the specimens was observed with an increase in the CIP contents, and the specimens incorporating 300% of CIP exhibited outcomes of 2.6 GHz and 0.4 GHz at bandwidths of −20 dB and −25 dB, respectively.
(3) It was found that the Fe atomic component in the specimens existed at rates of 0%, 0.34%, 0.73%, and 1.30% when the incorporated CIP contents were 0%, 100%, 200% and 300%, respectively, leading to an improvement of the EMI shielding capability of the specimens.
(4) The fabricated CIP-embedded CFRP composites were coated onto a cement mortar specimen and their EMI shielding capability was investigated, showing EMI shielding capabilities exceeding 50 dB at frequencies of 1 GHz and 2 GHz.

Declaration of Competing Interest

The authors declare that they have no known competing financial interests or personal relationships that could have appeared to influence the work reported in this paper.

Acknowledgments

This study was supported by a grant from the National Research Foundation of Korea (NRF) (2021R1A2C3006382) funded by the Korean government.

References

[1] Lei X, Zhang X, Song A, Gong S, Wang Y, Luo L, et al. Investigation of electrical conductivity and electromagnetic interference shielding performance of Au@CNT/sodium alginate/polydimethylsiloxane flexible composite. Compos Part A Appl Sci Manuf 2020;130:105762.
[2] Zhao Xu, Xu L, Chen Q, Peng Q, Yang M, Zhao W, et al. Highly Conductive Multifunctional rGO/CNT Hybrid Sponge for Electromagnetic Wave Shielding and Strain Sensor. Adv Mater Technol 2019;4(9):1900443. https://doi.org/10.1002/admt.201900443.
[3] Kong L, Yin X, Xu H, Yuan X, Wang T, Xu Z, et al. Powerful absorbing and lightweight electromagnetic shielding CNTs/RGO composite. Carbon N Y 2019;145:61–6. https://doi.org/10.1016/j.carbon.2019.01.009.
[4] Al-Saleh MH, Sundararaj U. Electromagnetic interference shielding mechanisms of CNT/polymer composites. Carbon N Y 2009;47(7):1738–46. https://doi.org/10.1016/j.carbon.2009.02.030.
[5] Fan Y, Zhang L, Volski V, Vandenbosch GAE, Blanpain B, Guo M. Utilization of Stainless-steel Furnace Dust as an Admixture for Synthesis of Cement-based Electromagnetic Interference Shielding Composites. Sci Rep 2017;7:4–11. https://doi.org/10.1038/s41598-017-15779-7.
[6] Nam IW, Choi JH, Kim CG, Lee HK. Fabrication and design of electromagnetic wave absorber composed of carbon nanotube-incorporated cement composites. Compos Struct 2018;206:439–47. https://doi.org/10.1016/j.compstruct.2018.07.058.
[7] Wang Z, Zhang T, Zhou L. Investigation on electromagnetic and microwave absorption properties of copper slag-filled cement mortar. Cem Concr Compos 2016;74:174–81. https://doi.org/10.1016/j.cemconcomp.2016.10.003.
[8] Nam IW, Lee HK, Jang JH. Electromagnetic interference shielding/absorbing characteristics of CNT-embedded epoxy composites. Compos Part A Appl Sci Manuf 2011;42(9):1110–8.

[9] Wang D, Ding S, Li L, Han B. Electromagnetic properties of multi-layer graphenes filled cementitious composites. Mater. Res. Express 2019;6(4):045046. https://doi.org/10.1088/2053-1591/aafc3d.

[10] Kim Y-K, Kim J, Jang D, Kim S, Jung W. A Study on the Effects of Multiwall Carbon Nanotubes on Dynamic Stiffness of Hydrophilic-base Magnetorheological Gel. Curr Nanosci 2019;15(3):319–23. https://doi.org/10.2174/1573413714666181023144334.

[11] Jang D, Yoon HN, Nam IW, Lee HK. Effect of carbonyl iron powder incorporation on the piezoresistive sensing characteristics of CNT-based polymeric sensor. Compos Struct 2020;244:112260. https://doi.org/10.1016/j.compstruct.2020.112260.

[12] Jang D, Yoon HN, Seo J, Lee HK, Kim GM. Effects of silica aerogel inclusion on the stability of heat generation and heat-dependent electrical characteristics of cementitious composites with CNT. Cem Concr Compos 2021;115:103861. https://doi.org/10.1016/j.cemconcomp.2020.103861.

[13] Yoon HN, Jang D, Lee HK, Nam IW. Influence of carbon fiber additions on the electromagnetic wave shielding characteristics of CNT-cement composites. Constr Build Mater 2021;269:121238. https://doi.org/10.1016/j.conbuildmat.2020.121238.

[14] Khalid HR, Choudhry I, Jang D, Abbas N, Haider MS, Lee HK. Facile Synthesis of Sprayed CNTs Layer-Embedded Stretchable Sensors with Controllable Sensitivity. Polymers (Basel) 2021;13:1–6.

[15] Jang D, Yoon HN, Seo J, Park S, Kil T, Lee HK. Improved electric heating characteristics of CNT-embedded polymeric composites with an addition of silica aerogel. Compos Sci Technol 2021;212:108866. https://doi.org/10.1016/j.compscitech.2021.108866.

[16] Micheli D, Vricella A, Pastore R, Delfini A, Bueno Morles R, Marchetti M, et al. Electromagnetic properties of carbon nanotube reinforced concrete composites for frequency selective shielding structures. Constr Build Mater 2017;131:267–77. https://doi.org/10.1016/j.conbuildmat.2016.11.078.

[17] Chen Y, Bin ZH, Huang Y, Jiang Y, Zheng WG, Yu ZZ. Magnetic and electrically conductive epoxy/graphene/carbonyl iron nanocomposites for efficient electromagnetic interference shielding. Compos Sci Technol 2015;118:178–85. https://doi.org/10.1016/j.compscitech.2015.08.023.

[18] Wang H, Zhu D, Zhou W, Luo Fa. Effect of Multiwalled Carbon Nanotubes on the Electromagnetic Interference Shielding Properties of Polyimide/Carbonyl Iron Composites. Ind Eng Chem Res 2015;54(25):6589–95. https://doi.org/10.1021/acs.iecr.5b01182.

[19] Sedlacik M, Mrlik M, Babayan V, Pavlinek V. Magnetorheological elastomers with efficient electromagnetic shielding. Compos Struct 2016;135:199–204. https://doi.org/10.1016/j.compstruct.2015.09.037.

[20] Zhang Z, Chen X, Wang Z, Heng L, Wang S, Tang Z, et al. Carbonyl iron/graphite microspheres with good impedance matching for ultra-broadband and highly efficient electromagnetic absorption. Opt Mater Express 2018;8(11):3319.

[21] Sum YL, Rheinheimer V, Soong BH, Monteiro PJM. Effects of Cement Paste Enhanced with Iron-Based Magnetic Particles on an Embedded Small Resonator Antenna. Sci Rep 2017;7:1–7. https://doi.org/10.1038/s41598-017-15289-6.

[22] Jang DI, Yun GE, Park J-E, Kim Y-K. Designing an attachable and power-efficient all-in-one module of a tunable vibration absorber based on magnetorheological elastomer. Smart Mater Struct 2018;27(8):085009. https://doi.org/10.1088/1361-665X/aacdbd.

[23] Jang D, Farooq SZ, Yoon HN, Khalid HR. Design of a highly flexible and sensitive multi-functional polymeric sensor incorporating CNTs and carbonyl iron powder. Compos Sci Technol 2021;207:108725. https://doi.org/10.1016/j.compscitech.2021.108725.

[24] Khalid HR, Nam IW, Choudhry I, Zheng L, Lee HK. Piezoresistive characteristics of CNT fiber-incorporated GFRP composites prepared with diversified fabrication schemes. Compos Struct 2018;203:835–43. https://doi.org/10.1016/j.compstruct.2018.08.003.

[25] Aly K, Li A, Bradford PD. Strain sensing in composites using aligned carbon nanotube sheets embedded in the interlaminar region. Compos Part A Appl Sci Manuf 2016;90:536–48. https://doi.org/10.1016/j.compositesa.2016.08.003.

[26] Salski B, Gwarek W, Korpas P, Reszewicz S, Chong AYB, Theodorakeas P, et al. Non-destructive testing of carbon-fibre-reinforced polymer materials with a radio-frequency inductive sensor. Compos Struct 2015;122:104–12. https://doi.org/10.1016/j.compstruct.2014.11.056.

[27] Nam IW, Lee HK. Synergistic effect of MWNT/fly ash incorporation on the EMI shielding/absorbing characteristics of cementitious materials. Constr Build Mater 2016;115:651–61. https://doi.org/10.1016/j.conbuildmat.2016.04.082.

[28] Park J-E, Yun G-E, Jang D-I, Kim Y-K. Analysis of Electrical Resistance and Impedance Change of Magnetorheological Gels with DC and AC Voltage for Magnetometer Application. Sensors 2019;19:2510. https://doi.org/10.3390/s19112510.

[29] Greenhoe BM, Hassan MK, Wiggins JS, Mauritz KA. Universal power law behavior of the AC conductivity versus frequency of agglomerate morphologies in conductive carbon nanotube-reinforced epoxy networks. J Polym Sci Part B Polym Phys 2016;54(19):1918–23. https://doi.org/10.1002/polb.24121.

[30] Jang D, Kil T, Yoon HN, Seo J, Khalid HR. Artificial neural network approach for predicting tunneling-induced and frequency-dependent electrical impedances of conductive polymeric composites. Mater Lett 2021;302:130420. https://doi.org/10.1016/j.matlet.2021.130420.

[31] Zhang L, Li L, Wang Y, Yu X, Han B. Multifunctional cement-based materials modified with electrostatic self-assembled CNT/TiO2 composite filler. Constr Build Mater 2020;238:117787. https://doi.org/10.1016/j.conbuildmat.2019.117787.

[32] Abbas SM, Chandra M, Verma A, Chatterjee R, Goel TC. Complex permittivity and microwave absorption properties of a composite dielectric absorber. Compos Part A Appl Sci Manuf 2006;37(11):2148–54.

[33] Afghahi SSS, Jafarian M, Atassi Y. A promising lightweight multicomponent microwave absorber based on doped barium hexaferrite/calcium titanate/multiwalled carbon nanotubes. J Nanoparticle Res 2016;18:1–11. https://doi.org/10.1007/s11051-016-3499-6.

[34] Park G, Kim S, Park G-K, Lee N. Influence of carbon fiber on the electromagnetic shielding effectiveness of high-performance fiber-reinforced cementitious composites. J Build Eng 2021;35:101982. https://doi.org/10.1016/j.jobe.2020.101982.

[35] Jang D, Park J-E, Kim Y-K. Evaluation of (CNT@CIP)-Embedded Magneto-Resistive Sensor Based on Carbon Nanotube and Carbonyl Iron Powder Polymer Composites. Polymers (Basel) 2022;14:542. https://doi.org/10.2307/j.ctvcm4g8n.8.

[36] Jang D, Yoon HN, Seo J, Yang B. Effects of exposure temperature on the piezoresistive sensing performances of MWCNT-embedded cementitious sensor. J Build Eng 2022;47:103816. 10.1016/j.jobe.2021.103816.

[37] Jang D, Yoon HN, Yang B, Seo J, Farooq SZ, Lee HK. Synergistic effects of CNT and CB inclusion on the piezoresistive sensing behaviors of cementitious composites blended with fly ash. Smart Struct Syst 2022;2:351–9.

[38] Manan Bhandari, Wang Jianchao, Jang Daeik, IlWoo Nam BH. A Comparative Study on the Electrical and Piezoresistive Sensing Characteristics of GFRP and CFRP Composites with Hybridized Incorporation of Carbon Nanotubes, Graphenes, Carbon Nanofibers, and Graphite Nanoplatelets. Sensors 2021;21:7291.

[39] Jang D, Yoon HN, Farooq SZ, Lee HK, Nam IW. Influence of water ingress on the electrical properties and electromechanical sensing capabilities of CNT / cement composites. J Build Eng 2021;42:103065. 10.1016/j.jobe.2021.103065.

[40] Kil T, Jang DI, Yoon HN, Yang B. Machine Learning-Based Predictions on the Self-Heating Characteristics of Nanocomposites with Hybrid Fillers. Comput Mater Contin 2022;71. 10.32604/cmc.2022.020940.